

Carbonate from the apatite of a Lehner mammoth tooth (A-876C) was younger than that from bone by 2000 years, which indicates that tooth apatite is less stable than bone apatite under the geochemical conditions at the Lehner site. It will be surprising if this turns out to be true generally, because tooth enamel is more dense than bone and therefore believed to be less subject to replacement or exchange by diffusion of solutions. On the other hand, the apparent difference in age could be due to differences in permeability between the sedimentary matrices of the bone and tooth, where the tooth was in a coarser, more permeable sediment than the bone was.

At the Hell Gap, Wyoming, site of early man, bone (probably bison) was collected from an archeological horizon that is correlated with a similar unit nearby that has been dated at  $8600 \pm 380$  years old (A-501) (3, p. 15). Both the collagen date (A-753A) and the bone apatite date (A-753C<sub>3</sub>) are in statistical agreement with each other and with the correlated date, which indicates that carbonate from the bone apatite is indeed indigenous. The calcium carbonate was hydrolyzed in two stages; the resulting dates (A-753C<sub>1</sub> and A-553C<sub>2</sub>) clearly indicate it to be secondary. The difference in age is probably caused by the fact that the outermost layers of secondary carbonate are the youngest and the first to be attacked by acid during hydrolysis.

The Murray Springs bovid bone is from a sedimentary unit that is believed to be between 50 and 500 years old. All the organic fractions show a slightly post-thermonuclear age (1960), which suggests contamination from bomb-produced C<sup>14</sup>. This interpretation is supported by the result of the calcium carbonate analysis (A-819C):  $125 \pm 5$  percent of the C<sup>14</sup> content of the modern standard. However, because the buried bovid skeleton is known to be of pre-nuclear age and because there was a 2.5-percent increase in the atmospheric C<sup>14</sup> budget approximately 250 years ago (7), I believe that the yearling lived within a few years of A.D. 1700. Unfortunately, the bone apatite fraction has not been analyzed.

From the research reported here it is concluded that the inorganic carbon of fossil bone is in two separate mineral phases, one of which (calcium carbonate) is of secondary origin, whereas the other (bone apatite) is indigenous. Collagen free of secondary organic matter and bone apatite free of calcium

carbonate can yield reliable radiocarbon dates, but contamination by insoluble noncollagenous organic matter (for example, saprophytes) and exchanged carbonates in bone apatite cannot always be precluded. Agreement between analysis of the two fractions is probably reasonable, but not conclusive, assurance that the radiocarbon age is correct.

VANCE HAYNES

Department of Geochronology,  
University of Arizona, Tucson

#### References and Notes

1. C. V. Haynes, in *Radioactive Dating and Methods of Low-Level Counting* (Intern. Atomic Energy Agency, Vienna, 1967), p. 163.
2. E. A. Olson, thesis, Columbia University (1963).
3. C. V. Haynes, P. E. Damon, D. C. Grey, *Radiocarbon* 8, 6 (1966).
4. D. McConnell, *Science* 136, 241 (1962); *Clin. Orthop.* 23, 253 (1962); *Amer. Mineral.* 45, 209 (1960); G. P. Brophy and T. M. Hatch, *ibid.* 47, 1174 (1962); R. Z. LeGeros, O. R. Trautz, J. P. LeGeros, E. Klein, W. P. Shirra, *Science* 155, 1409 (1967).
5. E. W. Haury, E. B. Syles, W. W. Wasley, *Amer. Antiquity* 25, 2 (1959).
6. It should be understood that if the calcium carbonate CO<sub>2</sub> is to be analyzed for radiocarbon it should not be hydrolyzed with acetic acid because the organic vapor could provide an extraneous source of CO<sub>2</sub> during its passage over the hot copper oxide used in most purification systems. Instead the calcium carbonate for analysis is hydrolyzed in a mineral acid on the assumption that it will hydrolyze at a much faster rate than the bone apatite. Results bear out this assumption.
7. P. E. Damon, A. Long, D. C. Grey, *J. Geophys. Res.* 71, 1055 (1966).
8. Radiocarbon dating and geological investigations supported by NSF grant GP-5548. Lehner mammoth tooth specimen provided by J. F. Lance and apatite specimens by J. W. Anthony, University of Arizona, Department of Geology. I thank P. E. Damon and R. H. Thompson for constructive criticism of the manuscript, and D. C. Grey and I. Zarins for their help in the radiocarbon laboratory. Contribution No. 168 of the University of Arizona Program in Geochronology.

14 May 1968

#### Seismic and Bathymetric Evidence of a Fracture Zone on Gorda Ridge

*Abstract. Swarms of seaquakes have been located hydroacoustically on Gorda Ridge near 41.5°N, 127.6°W, where detailed bathymetric charts indicate a slight dextral offset of the rift valley in the center of the ridge. It is suggested that a fracture zone may be nascent in the area.*

Recent work has shown that smaller submarine earthquakes (seaquakes) are located hydroacoustically than by the existing land-based seismographic network (1). During the years 1965 through 1967, seaquakes have been

routinely located in the Pacific Ocean Basin from arrival times of earthquake T-phases at hydrophones placed in the deep-ocean SOFAR (Sound Fixing And Ranging) channel at Eniwetok, Wake, Midway, and Oahu islands and off California (2); in the eastern Pacific most of those located were on the East Pacific Rise. The accuracy of location, relative to published earthquake epicenters (3), depends on the source-receiver geometry, accuracy of reading of arrival times, and knowledge of sound speed in the SOFAR channel. In the area of Gorda Ridge off the coasts of Washington and Oregon, location of sources by T-phase is especially good because the phones are distributed about the source, a nearby detection hydrophone off Cape Mendocino was used, and sound speed in the SOFAR channel is well known.

Epicentral times of earthquakes located by the U.S. Coast and Geodetic Survey on Gorda Ridge, Blanco Fracture Zone, and Juan de Fuca Ridge were compared with those of the corresponding T-phase source times; there was a mean difference of 5 seconds, with a standard deviation of 24 seconds, for 70 events between August 1965 and December 1966. (A 5-second error in time of origin means an error in location of about 7.3 km when a sound speed of 1.47 km/sec is used.) These epicenters were plotted on a large-scale (1:828,000) chart along with 955 additional epicenters located by T-phase that were presumably too low in magnitude to be detected by the Survey (which routinely locates earthquakes of magnitude 4 or greater). This plot was then laid over a detailed topographic map of the area. Figure 1 shows the Gorda Ridge section, scene of 78 percent of the epicenters located by T-phase. The epicenters are in two major zones: (i) a north-trending belt between 41° and 43°N, near 127.5°W; and (ii) a northwest-trending belt between 43° and 45°N and between 127° and 130°W. These seismic belts correspond to Gorda Ridge and Blanco Fracture Zone, respectively, as defined on the basis of bathymetry (4, 5). Thus, as has been demonstrated (6), the earthquakes are not restricted to fracture zones.

The greatest concentration of epicenters is at 41.5°N, 127.6°W. South of this cluster the epicenters are in the central rift valley [Escanaba Trough (5)] of Gorda Ridge. North of the cluster, epicenters occur along a line trend-

ing northeastward to the east end of Blanco Fracture Zone. The central rift valley is broken into a series of more or less closed basins near 41.5°N, whereas it is a prominent linear feature from there southward to Mendocino Fracture Zone (5). North of 41.5°N the central rift valley is displaced about 20 km eastward, and the trend of Gorda Ridge changes from nearly northward to north-northeastward. Both the positive magnetic anomaly and the negative gravity anomaly associated with the axis of the ridge are offset to the same degree and in the same direction as the topography (5, 7). It is along the line separating these two sections of Gorda Ridge that the new fracture zone postulated by McManus (5) may be forming. The indicated movement is right lateral, as would be expected (4), because both Blanco Fracture Zone to the north and

Mendocino Fracture Zone to the south have left-lateral displacement.

Release of elastic strain, which is proportional to the square root of seismic wave energy (8), may be calculated from the equation

$$\log J = 9 + 1.8M \quad (1)$$

where  $J$  is the energy in ergs and  $M$  is earthquake magnitude on the Richter scale. For studies of seaquakes the T-phase strength  $S$  (2) may be substituted in Eq. 1 as a function of earthquake magnitude; for example

$$S(db) = 20M - 51 \quad (2)$$

This formula assumes a slope of 20 db per unit of earthquake magnitude because T-phase strength is the logarithm of power level, and earthquake magnitude is the logarithm of amplitude (2). An intercept of  $-51$  is the least-squares fit to 92 earthquakes in this region,

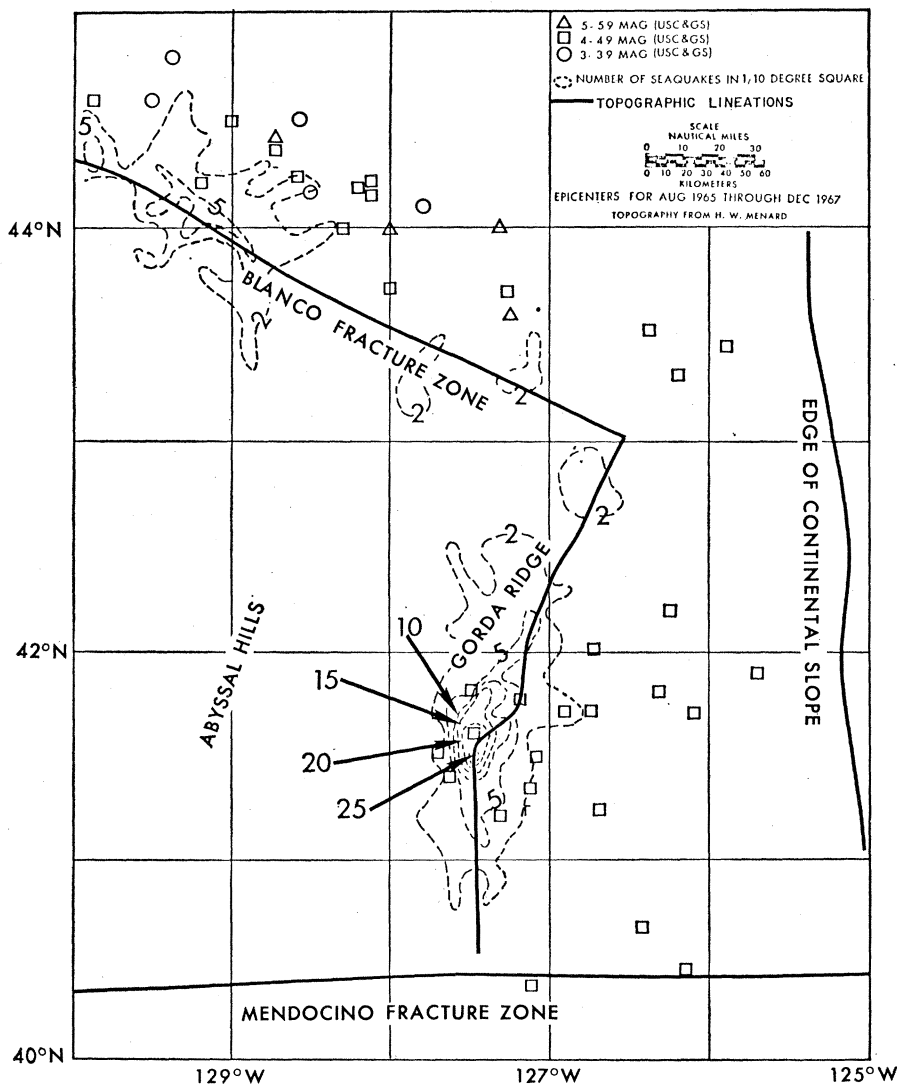


Fig. 1. Seismicity and bathymetry of Gorda Ridge. Seismicity shown by contours is based on the number of epicenters per 0.1-deg square.

16 AUGUST 1968

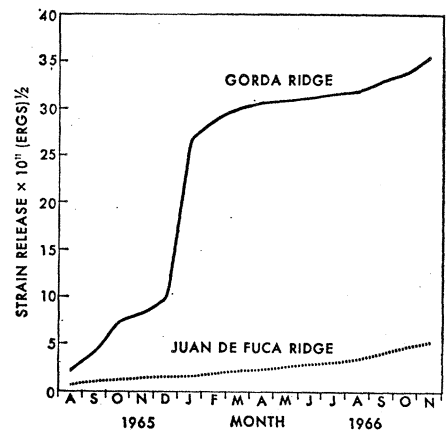


Fig. 2. Release of elastic strain, based on T-phase strength, for Gorda Ridge and Juan de Fuca Ridge. Data are for the period August 1965 through December 1966.

with a standard deviation of 10.3 db. With these relations the cumulative value of the square root of  $J$ , plotted against time (Fig. 2), gives an indication of the release of strain along Gorda Ridge and Blanco Fracture Zone for the 16-month period examined. Strain release along Juan de Fuca Ridge, north of 48°N, also is shown (Fig. 2) for comparison. No seaquakes were located on the southern part of Juan de Fuca Ridge, which appears to be aseismic (5).

The contribution of low-magnitude (lower than magnitude 4) earthquakes to the overall seismicity of the ridge is small, but a swarm of such earthquakes (as in January and February 1966) indicates unusual local seismicity along a disturbed zone. More earthquakes, then, occurred along fracture zones than on the crest of the ridge, but they were not restricted to the fracture zone.

Crustal layers involved in the faulting may be deduced from focal depths of earthquakes. However, present techniques provide no accurate method of determining focal depths from T-phase recordings, and the Survey lists the focal depth of almost all seaquakes as 33 km. The true focal depth is probably near 5 km (9), and normal faulting also may occur (10).

J. NORTHROP

Naval Undersea Warfare Center,  
San Diego Division,  
San Diego, California 92152

H. W. MENARD

University of California at San Diego,  
La Jolla 92037

F. K. DUENNEBIER

Hawaii Institute of Geophysics,  
Honolulu 96822

References and Notes

1. R. H. Johnson, J. Northrop, R. A. Eppley, *J. Geophys. Res.* **68**, 4251 (1963).
2. R. H. Johnson, *Bull. Seismol. Soc. Amer.* **56**, 109 (1966).
3. Located by the U.S. Coast and Geodetic Survey.
4. H. W. Menard, *Science* **155**, 72 (1966).
5. D. A. McManus, *Bull. Geol. Soc. Amer.* **78**, 527 (1967).
6. L. R. Sykes, *J. Geophys. Res.* **72**, 1231 (1967).
7. P. Dehlinger, R. W. Couch, M. Gemperle, *ibid.*, p. 1233.
8. H. Benioff, *Bull. Seismol. Soc. Amer.* **41**, 31 (1955).
9. J. N. Brune, *J. Geophys. Res.* **73**, 777 (1968).
10. T. M. Atwater and J. D. Mudie, *Science* **159**, 729 (1968).
11. Supported by Naval Undersea Warfare Center, San Diego Division; the Advanced Research Projects Agency; and the Office of Naval Research. We thank R. Parker and R. H. Johnson for help.

10 June 1968

**Magnesium Sulfate Interactions in Seawater from Solubility Measurements**

Abstract. *The extent of association between magnesium and sulfate ions was determined in artificial seawater by a solubility technique. About 10 percent of the magnesium ions were found to be associated. This result supersedes the earlier value found in this laboratory and agrees with the results of Garrels and Thompson, Thompson, and Fisher.*

Several researchers determined the extent of association between magnesium and sulfate ions in seawater. Garrels and Thompson, Thompson, and Fisher (1) found that between 9 and 11 percent of the magnesium ions are associated to sulfate ions. The results of Pytkowicz *et al.* (1) indicated that the extent of association was greater. In the present work we redetermined the extent of association, again by a method based on the solubility of brucite, and obtained results that agree with those of the other workers. The present procedure, in contrast to our previous one, avoided both the use of a value for the thermodynamic solubility product of brucite and the possibility of carbonate coprecipitation. Particle size effects were minimized because a comparative technique was used.

The procedure was as follows. Two solutions, with compositions shown in Table 1, were equilibrated with 40- to 60-mesh white platy Quebec brucite and the steady-state pH was measured at 25° ± 0.1°C. The pH measurements were made with an Orion model 801 digital pH meter, with a precision of

± 0.002 pH units. Solution B, with the exception of carbonate and borate which were not added in its preparation, corresponds to seawater of 34.8 parts per mille salinity. The absence of carbonate in the two solutions was necessary to avoid either the precipitation of calcium carbonate which could affect the final pH or the possible alteration of the brucite surface by carbonate inclusion. Fresh samples of brucite were prepared and washed with distilled water before each pair of runs in solutions A and B. Preliminary measurements had shown that the same final pH was obtained either with immersion of the glass electrode into the brucite or with stirring of the solution and of the solid. The immersion technique was used in subsequent experiments because it permitted faster equilibration.

The calculations were based on the following equations. The thermodynamic solubility product of brucite is the same in solutions A and B. Therefore:

$$(a_{Mg})_A (a_{OH})^2_A = (a_{Mg})_B (a_{OH})^2_B \quad (1)$$

For a given solution, the following equation, discussed by Pytkowicz *et al.* (1), is valid:

$$a = f_F (F) = f_T (T) \quad (2)$$

where *a* is the activity, *f* is the activity coefficient, the parentheses represent molalities, *F* indicates free quantities,

and *T* indicates total (free plus associated) quantities. From Eqs. 1 and 2 it follows that

$$\frac{(a_{OH})^2_A}{(a_{OH})^2_B} = \frac{(f_{Mg})_{BF} (Mg^{2+})_{BF}}{(f_{Mg})_{AF} (Mg^{2+})_{AF}} \quad (3)$$

The subscripts *AF* and *BF* represent the free ions in solutions A and B respectively.

Solutions A and B had the same stoichiometric ionic strength, that is, the stoichiometric ionic strength corrected for ion association. For solution A, which consists only of chlorides, there should be no ion association (2). For solution B the extent of association was estimated from the model of Garrels and Thompson (1). An assumption in the ion association model is that free activity coefficients depend only on the effective ionic strength and not on the composition of the medium. The adequacy of this assumption was verified by Pytkowicz and Kester (3) for sodium ions upon replacement of chloride by sulfate ions at constant effective ionic strength. It is likely, therefore, that  $(f_{Mg})_{BF} = (f_{Mg})_{AF}$ .

The absence of chloride ion association means that  $(Mg^{2+})_{AF} = (Mg^{2+})_{AT}$ , where the subscript *AT* refers to the total concentration in solution A. Also, the thermodynamic dissociation constant of water is the same in the two solutions. Therefore, Eq. 3 can be reduced to

$$(Mg^{2+})_{BF} = (Mg^{2+})_{AT} \frac{(a_H)^2_B}{(a_H)^2_A} \quad (4)$$

Thus,  $(Mg^{2+})_{BF}$ , the concentration of free magnesium ions in solution B, may be obtained from the stoichiometric concentration of magnesium and from the values of the steady-state pH at equilibrium with brucite in solutions A and B. The concentration of  $MgSO_4^0$  ion pairs is obtainable from

$$(MgSO_4)_B = (Mg^{2+})_{BT} - (Mg^{2+})_{BF} \quad (5)$$

*BT* indicates the total concentration in solution B.

Table 1. Ionic concentrations of the solutions.

Ion	Concentration (molal units)	
	Solution A	Solution B
Na	0.473	0.482
Mg	.0548	.0548
Ca	.0106	.0106
K	.0102	.0102
Sr		.00009
Cl	.614	.564
SO <sub>4</sub>		.0291
Br		.00086
F		.00005

Table 2. Steady-state pH, free magnesium ion concentration, concentration of  $MgSO_4^0$  ion pairs, and percent of magnesium ions associated to sulfate ions at 25°C and 34.8 per mille salinity.

Run	Steady-state pH		$(Mg^{2+})_{BF}$	$(MgSO_4^0)$	Associated magnesium (percent)
	Solution A	Solution B			
1	9.314	9.335	0.0493	0.0055	10
2	9.287	9.314	.0482	.0066	12
3	9.308	9.328	.0499	.0049	9
Average					10